

Optimal demonstration of Autler–Townes splitting

Yang Dong,^{1,2} Yu Zheng,^{1,2} Xiang-Dong Chen,^{1,2} Guang-Can Guo,^{1,2} and Fang-Wen Sun^{1,2,*}

¹*CAS Key Lab of Quantum Information, University of Science and Technology of China, Hefei, 230026, P.R. China*

²*Synergetic Innovation Center of Quantum Information & Quantum Physics,
University of Science and Technology of China, Hefei, 230026, P.R. China*

(Dated: December 14, 2017)

The atom-light interaction in a three-level system has shown significant physical phenomena, such as electromagnetically induced transparency and Autler–Townes splitting (ATS), for broad applications in classical and quantum information techniques. Here, we optimally demonstrated the ATS with a quantum state manipulation method. The ATS in the dephasing-dominated diamond NV center system was successfully recovered by coherent microwave control, which cannot be observed with traditional method. The dynamical process of ATS was investigated in detail, revealing a non-trivial quantum interference with geometric phase modulations. Based on the quantum interference, the signal of the optimal ATS is twice as intense as those with traditional observation method.

I. INTRODUCTION

Atom-light interaction is a fundamental topic in quantum optics and atomic physics. In this realm, the optical response of the quantum multilevel system can be dramatically modified by quantum interferences among different transition pathways, or by the strong Stark effect [1]. As a typical representative of the former, electromagnetically induced transparency (EIT) [2–4] can create an ultra-narrow transparency window and delicately control the absorption and dispersion of the medium, and thus many remarkable applications are being explored [2–4]. The Stark effect also creates a transparency window because of the doublet splitting structure in the absorption spectrum, which is called Autler–Townes splitting (ATS). ATS has been employed to measure transition dipole moments [5], to control the spin-orbit interaction in quantum system [6], to suppress quantum decoherence [7–10], to dynamically control resonance fluorescence spectra [11] and to create disorder for time crystals [12]. In the last two decades, many systems have been used to investigate EIT and ATS, such as atoms [6, 13], superconducting systems [14–16], quantum dots [17–21], defects in diamond [9, 19–22], and nano-photonic systems [23–27].

Until now, almost all studies of EIT and ATS have been performed on atomic-like system based on the traditional spectral-domain observational method with long-duration driving (coupling and probe) pulses [5–11, 15, 16, 18, 27], wherein quantum decoherence is dominated by the longitudinal relaxation process [2–4]. However, with recent developments in materials science [28–31], rapid pure dephasing processes dominate the quantum decoherence, such as in solid spin systems and superconducting systems [29]. In these systems, when the driving pulses is much longer than the dephasing time, the quantum coherence is lost and the EIT and ATS phenomena disappear. Hence, the traditional observation

method imposes a serious restriction on the investigation and application of both phenomena. In this Letter, we optimally demonstrated the ATS by applying the quantum state manipulation [32, 33] method. The ATS was successfully recovered in diamond nitrogen vacancy (NV) center system where the quantum decoherence is dominated by the dephasing process [28–31].

The diamond NV center has been one of promising candidates for quantum information processes. Many studies have successfully demonstrated one-, and multi-qubit coherent operations [34–37] at room-temperature. Using the electron spin triplet state of the NV center, the V-type quantum three-level system can be directly obtained. With the quantum state manipulation method, ATS is observed in such a dephasing dominated system and the dynamic process of ATS is investigated in detail by controlling the pulse sequence. A nontrivial oscillation driven by the probe and coupling field was experimentally revealed, including both geometric phase and quantum interference in this three-level coupling. This dynamic behavior is notably different from that of a two-level system with Rabi oscillation. Moreover, with delicately control of the interference and geometric phase, the signal intensity of ATS is twice that the traditional method due to quantum interference, which is the optimal demonstration of ATS.

II. RECOVERY OF ATS

The NV center consists of a substitutional nitrogen atom adjacent to a carbon vacancy, and the ground state exhibits zero-field splitting between the $m_s = 0$ and degenerate $m_s = \pm 1$ sub-levels of $D \approx 2.87$ GHz [38, 39]. The spin-dependent photon luminescence (PL) enables the implementation of optically detected magnetic resonance (ODMR) techniques [39] to detect the spin state with normalized $PL_{m_s=0} = 1$ and $PL_{m_s=\pm 1} \approx 0.78$ in the current experiment. With secular approximation, the effective Hamiltonian of the ground state triplet of the

* fwsun@ustc.edu.cn

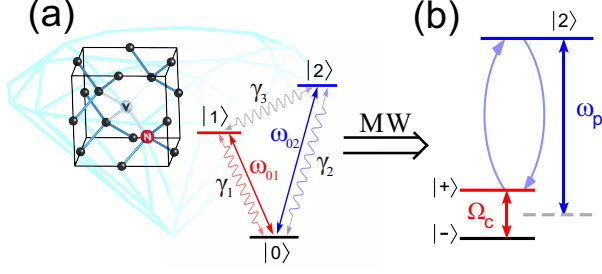


FIG. 1. (a) V-type three levels of the NV center ground state. The degenerated $m_s = \pm 1$ sublevels are removed by applying a static magnetic field. The dephasing rates of each level are γ_1 , γ_2 , and γ_3 . (b) Energy levels under a strong coupling field. $|+\rangle = (|0\rangle + |1\rangle)/\sqrt{2}$ and $|-\rangle = (|0\rangle - |1\rangle)/\sqrt{2}$ are separated by Ω_c . The $|+\rangle \leftrightarrow |2\rangle$ transition is selected to study the dynamical process of the ATS.

NV center [38],

$$H = DS_z^2 - \gamma_e B_z S_z, \quad (1)$$

is defined by the Zeeman splitting with the external magnetic field B_z along the electron spin S_z , and γ_e is the electron gyromagnetic ratio. As a result, the V-type three-level system is formed with the states $|0\rangle \equiv |m_s = 0\rangle$, $|1\rangle \equiv |m_s = -1\rangle$ and $|2\rangle \equiv |m_s = +1\rangle$, where $\omega_{0,1}$ ($\omega_{0,2}$) is the transition frequency between $|0\rangle$ and $|1\rangle$ ($|2\rangle$), as shown in Fig.1(a).

When microwave (MW) coupling (ω_c) and probe (ω_p) fields are applied to drive the NV center, the Hamiltonian of ATS with the rotating-wave approximation is

$$H_{ATS} = \begin{bmatrix} 0 & \frac{\Omega_c}{2} & \frac{\Omega_p}{2} \\ \frac{\Omega_c}{2} & \Delta_c & 0 \\ \frac{\Omega_p}{2} & 0 & \Delta_p \end{bmatrix}, \quad (2)$$

where $\Delta_c = \omega_c - \omega_{0,1}$ ($\Delta_p = \omega_p - \omega_{0,2}$) is the frequency detuning between the coupling (probe) field and the transition between $|0\rangle$ and $|1\rangle$ ($|2\rangle$). Correspondingly, Ω_c and Ω_p are Rabi oscillation frequencies for the coupling and probe fields, respectively. When the coupling field is resonant with its corresponding transition ($\Delta_c = 0$) and much stronger than the probe field, the eigen-energy levels are split by $\pm\Omega_c/2$ with eigenstates $|+\rangle = (|0\rangle + |1\rangle)/\sqrt{2}$ and $|-\rangle = (|0\rangle - |1\rangle)/\sqrt{2}$, as shown in Fig.1(b). For an atomic-like system, the quantum decoherence is dominated by the longitudinal relaxation process such as spontaneous radiation. The system will be in eigenstates with long-duration driving pulses. When the frequency of the probe field is scanned, two absorption peaks can be observed after the probe field is resonant with the eigenenergy levels [10, 11, 40], thus presenting ATS. This is the traditional method based on the spectral measurement. However, for single NV center in bulk diamond with the natural ^{13}C isotope, the dephasing process ($\sim 10 \mu\text{s}$), which is caused by interaction with a nuclear spin bath [38, 41], is much faster than the

longitudinal depolarization process ($\sim 2 \text{ ms}$) [42]. Thus when the driving pulse is much longer than the dephasing time, the dephasing dominated system would be in the maximally mixed state $(|0\rangle\langle 0| + |1\rangle\langle 1| + |2\rangle\langle 2|)/3$. The splitting would not be observed by scanning the probe field (see the Appendix for the theoretical calculation and simulation.).

In this experiment, to fully study the ATS with NV center, we employ the quantum state manipulation method, as shown in Fig.2. The electronic spin qubit was initialized into the $m_s = 0$ state by a $3 \mu\text{s}$ 532 nm optical pulse. At the proper magnetic field strengths (51 mT), optical pumping also polarizes the ^{14}N nuclear spin of the NV center into $m_I = +1$, because resonant polarization exchanges with the electron spin in the excited state. Then we simultaneously applied coupling and probe fields with an identical duration time. Finally, the electron spin state was read with another 532 nm optical pulse. When the duration time was set to be $t = 52.2 \mu\text{s}$, which was much longer than the dephasing time, no splitting was observed as the probe field was scanned. As shown in Fig.2(b), the PL was maintained at $(PL_{|0\rangle\langle 0|} + PL_{|1\rangle\langle 1|} + PL_{|2\rangle\langle 2|})/3 \approx 0.85$, which corresponded to the maximally mixed state. This result

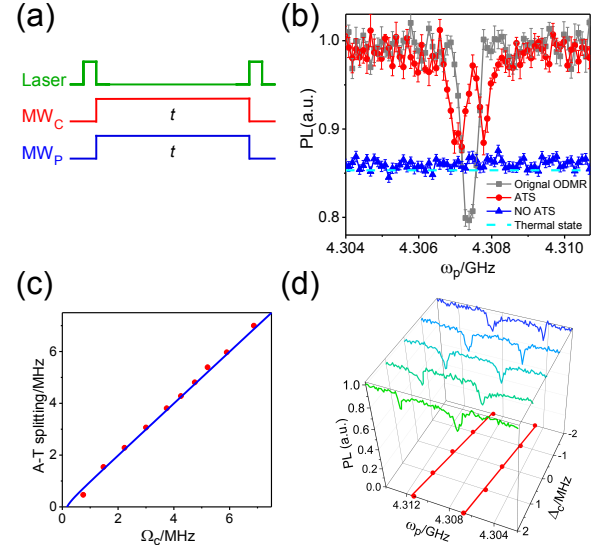


FIG. 2. (a) Optical and MW pulse sequences for the ATS experiment. Both coupling and probe fields are simultaneously applied with identical durations. (b) ODMR spectrum of the NV center. The blue triangles denote the traditional measurement result with long time driving pulses. No splitting was observed. The red dots denote the ATS. The cyan dashed line shows the PL of the maximal mixed state of the NV center. The gray squares show the $|0\rangle \leftrightarrow |2\rangle$ transition, which demonstrates the original ODMR spectrum without a coupling field. (c) ATS versus the amplitude of the coupling field with red dots. The blue curve is the theoretical result. (d) ATS versus the detuning of the couple field. In the bottom, the positions of the splitting are fitted by the theoretical model, as shown with the red solid line.

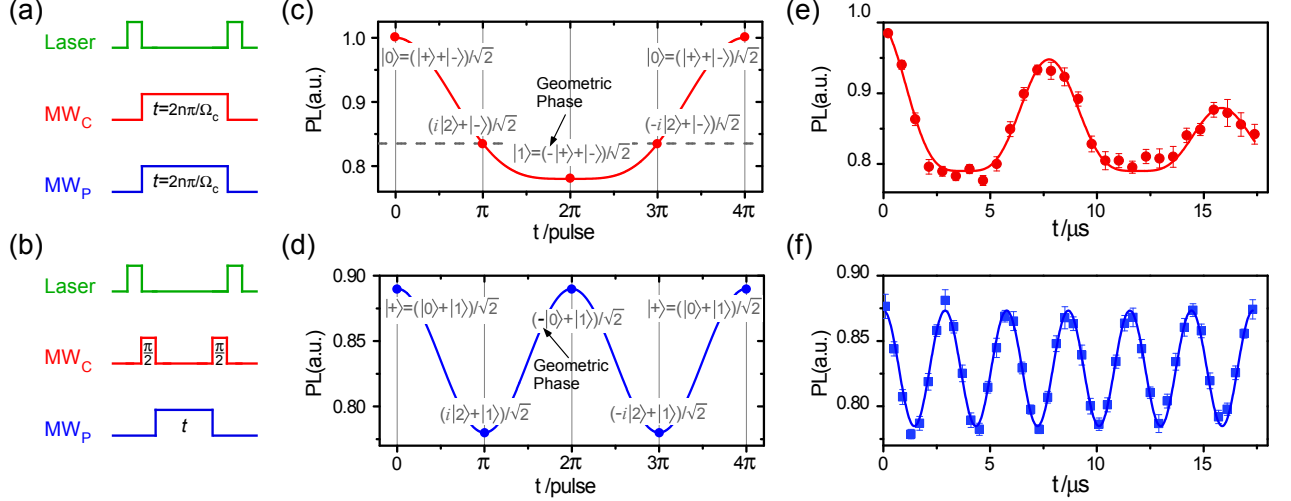


FIG. 3. (a) Optical and MW pulse sequences used to study the dynamical process of ATS. Both driving fields were simultaneously applied, and the duration time was set to $t = 2n\pi/\Omega_c$, with $\Omega_c = 2\pi \times 4.73(1)$ MHz and $\Omega_c/\Omega_p = 14$. (b) Optical and MW pulse sequences used for Rabi oscillation between $|+\rangle = (|0\rangle + |1\rangle)/\sqrt{2}$ and $|2\rangle$. The $\pi/2$ coupling pulse was used to generate $|+\rangle$. The probe field was resonantly applied to the transitions between $|+\rangle$ and $|2\rangle$. (c)(d) The diagrams of the transition between $|+\rangle$ and $|2\rangle$ with and without ATS. (e)(f) Experimental results of the transition between $|+\rangle$ and $|2\rangle$ with and without ATS. The Rabi frequency in (f) is $2.74(4) \approx 2\sqrt{2}$ of that in (e).

demonstrates that quantum dephasing has a disastrous effect on the investigation of ATS compare with the quantum longitudinal relaxation process.

However, if we control the duration time of the driving fields to $t = 1.8\mu s = \pi/\Omega_p = 2\pi/\Omega_c$, the doublet, which was spaced by the coupling Rabi frequency Ω_c , was observed to recover the ATS, as shown in Fig.2(b). To explain this result, we present the ATS dynamics based on Eq.(2) under the coupling field resonance with a single NV center, which is expressed as [10, 11]

$$H_d = \begin{bmatrix} \frac{\Omega_c}{2} & 0 & \frac{\sqrt{2}\Omega_p}{4} \\ 0 & -\frac{\Omega_c}{2} & \frac{\sqrt{2}\Omega_p}{4} \\ \frac{\sqrt{2}\Omega_p}{4} & \frac{\sqrt{2}\Omega_p}{4} & \Delta_p \end{bmatrix}, \quad (3)$$

where $|+\rangle$, $|-\rangle$ and $|2\rangle = |2\rangle$ form the new basis vectors. When $\Delta_p = 0$, the effect of the probe field can be neglected due to the large detuning between $|\pm\rangle$ and $|2\rangle$. The spin state is in $|0\rangle$ with the maximal PL. However, when $\Delta_p \approx \pm\Omega_c/2$, we can eliminate the transition matrix element between $|\mp\rangle$ and $|2\rangle$ using the second order perturbation theory. Hence, the probe field will drive the system to oscillate between $|\pm\rangle$ and $|2\rangle$ with lower PL, which demonstrates the ATS. Theoretically, the splitting frequency from Eq.(3) is $\Delta_{AT} = \Omega_c + \Omega_p^2/(4\Omega_c)$. In Fig.2(c), we independently measured the ATS as a function of the intensity of the coupling field (denoted by Rabi frequency Ω_c). Here, the observed ATS is almost equal to the Rabi frequency of the coupling field when $\Omega_c \gg \Omega_p$, which demonstrates the ATS characteristic. When the coupling field is not resonant, the doublet split dips are not symmetric, which can be attributed to the unbal-

anced superposition of $|0\rangle$ and $|1\rangle$, and the eigenenergies of the driven system are $E_{\pm} = \omega_{0,2} + \Delta_c/2 \pm \Omega_{eff}/2$, where $\Omega_{eff} = \sqrt{\Delta_c^2 + \Omega_c^2}$. As shown in Fig.2(d), when $\Delta_c \ll \Omega_c$, the positions of ATS approximately have a linear relationship with the detuning of the coupling field when the effect of the Rabi frequency (Ω_{eff}) remains unchanged.

III. DYNAMICAL PROCESS OF ATS

In addition to demonstrating splitting, we can study the dynamical process of ATS in detail. In the multi-level system, besides multiple separated transitions between different two levels, the quantum interference between those transitions shows a primary difference with the two-level system. Such quantum interference has been well demonstrated in EIT and usually believed to occur only in EIT. With the quantum state manipulation method, the quantum interference was also revealed with geometric phase modulations in ATS. In the experiment, the spin is first initialized into $|0\rangle$, which is the superposition of $|+\rangle$ and $|-\rangle$, i.e. $|0\rangle = (|+\rangle + |-\rangle)/\sqrt{2}$. When the probe field is resonant with the $|+\rangle \leftrightarrow |2\rangle$ transition by setting $\Delta_p \approx \Omega_c/2$, it will flop the population between $|+\rangle$ and $|2\rangle$ at a frequency $\Omega_{+,2} = \sqrt{2}\Omega_p/2$. When the state $|+\rangle$ is driven by a 2π probe pulse, it acquires a geometric phase $e^{-i\pi}$ [35, 43–45]. Simultaneously, the state $|-\rangle$ acquired a dynamical phase of $e^{i\Omega_c t}$ with the coupling field. If the pulse duration also satisfies $\Omega_c t = 2n\pi$ ($n = 1, 2, 3, \dots$) for $e^{i\Omega_c t} = 1$, the spin state is at $(-|+\rangle + |-\rangle)/\sqrt{2} = -|1\rangle$. In this case, another 2π probe

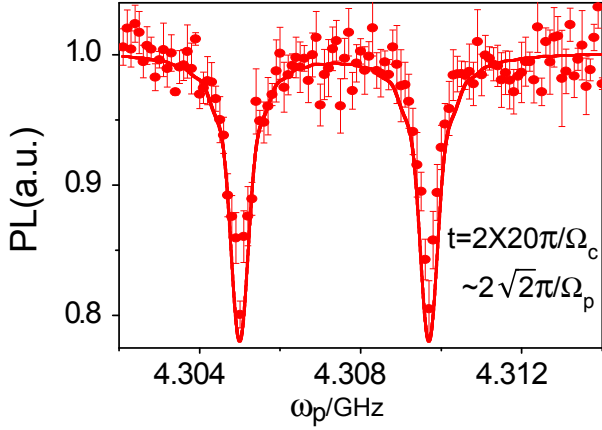


FIG. 4. Optimal demonstration of ATS with $t = 2 \times 20\pi / \Omega_c \approx 2\sqrt{2}\pi / \Omega_p$. The signal intensity (red dots) of the doublet dips is almost same as the original signal in Fig.2(b).

pulse would be required to reconvert to $|0\rangle$, as shown in Fig.3(c) with the pulses sequences in Fig.3(a). Hence, the geometrical phase doubles the driving duration time and halves the transition frequency. For comparison, Fig.3(d) shows the Rabi oscillation between $|+\rangle \leftrightarrow |2\rangle$ without the coupling field. In experiment, when the electron spin state is detected by the operator $|0\rangle\langle 0|$ with the ODMR method, Fig.3(c) and (d) also show the PL of the two dynamic processes. The Rabi frequency oscillation is Ω_p , whereas the ATS frequency is $\Omega_{+,2}/2 = \sqrt{2}\Omega_p/4$. This result can also be obtained by solving Eq.(3), where the population of $|0\rangle\langle 0|$ can be expressed as follows,

$$P_{|0\rangle\langle 0|} = \frac{1}{4} \left| \cos(\sqrt{2}\Omega_p t/4) + e^{i\Omega_c t} \right|^2. \quad (4)$$

This expression clearly demonstrates the quantum interference between $|+\rangle \leftrightarrow |2\rangle$ and $|-\rangle$. In the experiment to study the quantum interference with geometric phase modulations in ATS, we set $t = 2n\pi / \Omega_c$ with $\Omega_c / \Omega_p = 14$ and detected the spin-dependent PL. The experimental result is illustrated in Fig.3(e). Because of the dephasing processes, the data can be fitted by a theoretical curve $S(t) = ae^{-(t/T)^k} \cos^4[w(t - t_c)] + b$, where $a = 0.211(9)$, $T = 17.5(1) \mu\text{s}$, $k = 1.5(3)$, $t_c = 7.85(5) \mu\text{s}$, $b = 0.790(3)$ and the frequency $w = 2\pi \times 0.123(2) \text{ MHz}$. Correspondingly, the results of Rabi oscillation between $|+\rangle \leftrightarrow |2\rangle$ is shown in Fig.3(f) with the Rabi frequency of $\Omega_p = 2\pi \times 0.338(1) \text{ MHz}$. We can find $\Omega_p / \omega = 2.74(4) \approx 2\sqrt{2}$, which is consistent with the above theory.

IV. OPTIMAL DEMONSTRATION OF ATS.

The quantum state manipulation method is an optimal way to present the ATS with maximal signal intensity. Because of the quantum interference between $|+\rangle \leftrightarrow |2\rangle$

and $|-\rangle$, the ATS signal can be optimized when the duration time satisfies

$$\Omega_p t = 2\sqrt{2}(2k - 1)\pi, \quad \Omega_c t = 2n\pi, \quad (5)$$

or

$$\Omega_p t = 2\sqrt{2}(2k)\pi, \quad \Omega_c t = (2n - 1)\pi, \quad (6)$$

with $n, k = 1, 2, 3, \dots$. In this case, the system remains in $|1\rangle$, the NV center provides minimal photon luminescence, and the ATS exhibits the maximal dips. In the experiment, we set $t = 2 \times 20\pi / \Omega_c \approx 2\sqrt{2}\pi / \Omega_p$ with $\Omega_c / \Omega_p = 14$. By scanning the probe field, we can obtain the result in Fig.4. The depth of the ATS is almost same as original signal in Fig.2(b), because of the quantum interference of the three-energy-level systems. In contrast, for the traditional method [5–11, 15, 16, 18, 27], the signal intensity of ATS is only half of the original signal for lacking quantum interference with the third energy level. Therefore, such an enhancement in the signal with full control of quantum state in ATS may contribute to the precision measurement of the spectrum of a quantum system.

V. DISCUSSION

In conclusion, we have presented an optimal observation method based on quantum state manipulation to study and demonstrate ATS. The ATS was recovered in a dephasing-dominated quantum system, which can not be observed with traditional observation methods. With the quantum state manipulation methods, the dynamical process of ATS was investigated in detail with a nontrivial behavior from the quantum interference with geometric phase modulations. Consequently, the ATS was optimally demonstrated, and its signal intensity was twice those of other systems observed with the traditional observation method. The study presents a feasible method to optimally observe the atom-light interaction in a multi-level system, which can be applied to investigate quantum optics and atomic physics for a broad applications in high-dimensional quantum control and quantum error correction beyond the dynamically decoupling, decoherence-free subspace.

ACKNOWLEDGMENT

This work was supported by the National Key Research and Development Program of China (No. 2017YFA0304504), and the National Natural Science Foundation of China (Nos. 11374290, 61522508, 91536219, and 11504363).

Appendix A: Experimental setup and work point of the quantum system

1. Experimental setup

As shown in Fig.5, the NV center was located and detected with a home-built confocal microscopy with a dry objective lens ($N.A. = 0.95$) at room temperature. The power of 532 nm continuous laser was set at 0.6 mW. The NV center fluorescence was separated from the excitation laser with a 647 nm long pass filter and then detected by single photon counting modules. We constructed two synchronized microwaves that drove the NV center system with two different frequencies. The microwave was coupled to the sample by a coplanar waveguide.

Single photon emission from a single NV center was verified by measuring the photon correlation function $g^2(\tau)$ as shown in Fig.6(b). And $g^2(\tau) < 0.5$ indicates a single NV center. To form a simple V-type three-level system, a magnetic field of 51 mT was applied along the NV axis using a permanent magnet. Under this condition, the flip-flop process between electron-spin and nuclear-spin during optical pumping [39] leads to polarizing the nitrogen nuclear spin of NV center after 3 μ s green laser illumination. The Zeeman energy from the 51 mT magnetic field shifts the respective energy differences between $|0\rangle \equiv |m_s = 0\rangle \leftrightarrow |1\rangle \equiv |m_s = -1\rangle$ and $|0\rangle \leftrightarrow |2\rangle \equiv |m_s = 1\rangle$ from the zero-field splitting, 2.870 GHz, to 1.43398(1) GHz and 4.30738(1) GHz, as shown in Fig.6(c)-6(d).

2. Decoherence time

For single NV center, the electron spin states dephasing [28, 32, 38, 42] is the main part of quantum decoher-

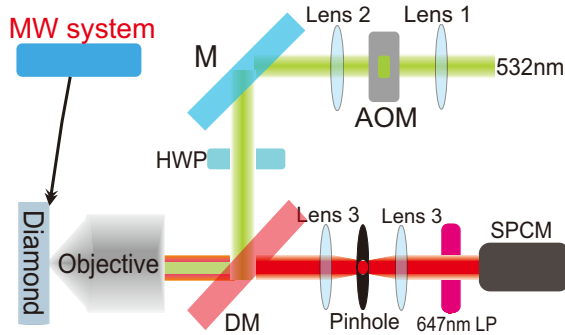


FIG. 5. Sketch of the experimental setup. Lens: optical lens with $f_1 = 100$ mm, $f_2 = 300$ mm and $f_3 = 30$ mm; AOM: acoustic optical modulator; M: mirror; HWP: half-wave plate for 532 nm laser; DM: long pass dichroic mirrors (DM) edge wavelength 536.8 nm. The pinhole ($d = 15$ μ m) and 647 nm long pass filter were used to filter stray light; SPCM: single photon counting module.

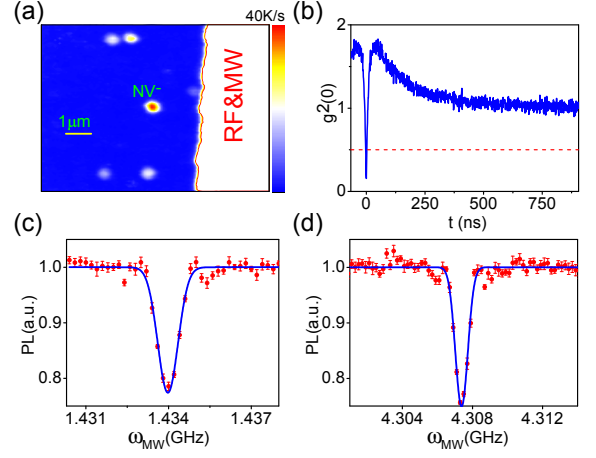


FIG. 6. (a) Confocal image of the NV center used in the experiment with a signal-to-noise ratio of 140:1. A coplanar waveguide antenna was deposited to deliver microwave pulses to the NV center. (b) Fluorescence correlation function. (c)-(d) ODMR spectra for the single NV center. The transition frequencies for $|0\rangle \rightarrow |1\rangle$ and $|0\rangle \rightarrow |2\rangle$ are $\omega_{0,-1} = 1.43398(1)$ GHz and $\omega_{0,1} = 4.30738(1)$ GHz, respectively.

ence and has an impact on the ATS. The dephasing time of NV center was measured by the Ramsey interferometer [38, 42]. By fitting experimental data as shown in Fig.S3(a), we got $T_{2,0\leftrightarrow 1}^* = 8.2(3)$ μ s and $T_{2,0\leftrightarrow 2}^* = 8.7(4)$ μ s. We also measured the resonant Rabi oscillation of NV center driven only by the probe or coupling field as shown in Fig.7(b)-(c). The Rabi frequency was kept same as in Fig.2 and $\Omega_c/\Omega_p = 2$. The damping times are $T_{1,p} = 25.0(8)$ μ s and $T_{1,p} = 9.5(5)$ μ s for $|0\rangle \leftrightarrow |1\rangle$ and $|0\rangle \leftrightarrow |2\rangle$, respectively, by fitting the data. After the depolarization time of NV center was measured as shown in Fig.7(d) with $T_1 = 1.7(2)$ ms, we confirmed that the dephasing process, which caused by nuclear spin bath, dominated the quantum decoherence of NV center.

Appendix B: Theoretical model of the ATS with quantum state manipulation

The Hamiltonian for NV center under driving fields in experiment reads

$$H = \omega_{0,-1} |1\rangle \langle 1| + \omega_{0,1} |2\rangle \langle 2| + \Omega_c \cos(\omega_c t + \varphi_c) [|1\rangle \langle 0| + |0\rangle \langle 1|] + \Omega_p \cos(\omega_p t + \varphi_p) [|2\rangle \langle 0| + |0\rangle \langle 2|], \quad (B1)$$

where φ_c and φ_p are the initial phases of the coupling and probe fields, respectively.

After transforming to a frame co-rotating with the two driving fields via $U_0 = e^{iH_0 t}$ with $H_0 = \omega_c |1\rangle \langle 1| + \omega_p |2\rangle \langle 2|$, we get

$$H = \begin{pmatrix} 0 & \frac{\Omega_c}{2} e^{i\varphi_c} & \frac{\Omega_p}{2} e^{i\varphi_p} \\ \frac{\Omega_c}{2} e^{-i\varphi_c} & \Delta_c & 0 \\ \frac{\Omega_p}{2} e^{-i\varphi_p} & 0 & \Delta_p \end{pmatrix}. \quad (B2)$$

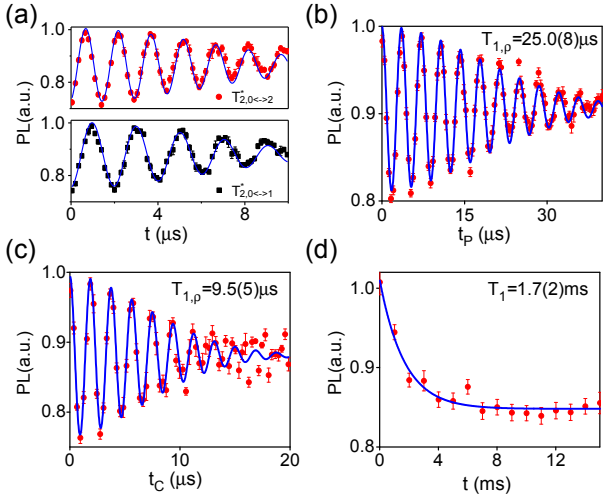


FIG. 7. (a) Result of the Ramsey experiment for the electron spin of NV center. Black squares and red circles correspond to $|0\rangle \leftrightarrow |1\rangle$ and $|0\rangle \leftrightarrow |2\rangle$, respectively. Experimental data are fitted by $y(t) = a \exp[-(t/T_2^*)^2] \cos(2\pi\omega t) + b$ and denoted with solid blue curves. The dephasing time of NV center was measured to be $T_{2,0 \leftrightarrow 1}^* = 8.2(3) \mu s$ and $T_{2,0 \leftrightarrow 2}^* = 8.7(4) \mu s$. (b)-(c) Rabi oscillation of the electron spin between ground state sublevels of NV center. The experimental data (red dots) was fitted by a damped sine function (blue curves) written as $y(t) = a \exp[-(t/T_{1,p})^2] \cos(\pi \frac{x-x_c}{w}) + b$. We can get $T_{1,p} = 25.0(8) \mu s$ ($9.5(5) \mu s$) for only the probe (coupling) field. (d) The depolarization process of NV center (red dots) was fitted by $y(t) = a \exp(-t/T_1) + b$ and we got $T_1 = 1.7(2) ms$.

1. The neglect of the initial phases of driving fields

After initializing the NV center into its ground state $|0\rangle$, we can apply quantum gate $U = e^{-iHt}$ operation. Hence, $|\psi\rangle = e^{-iHt} |0\rangle$. Finally, we detect the final state, which does not distinguish the states $|1\rangle \equiv |m_s = -1\rangle$ and $|2\rangle \equiv |m_s = 1\rangle$. So we can use the measurement operator $|0\rangle\langle 0|$ to describe the detection process

$$\begin{aligned} P_{|0\rangle\langle 0|} &= \text{tr}(|0\rangle\langle 0| |\psi\rangle\langle \psi|) \\ &= \langle 0| |\psi\rangle\langle \psi| |0\rangle \\ &= |\langle 0| VV^\dagger e^{-iHt} VV^\dagger |0\rangle|^2. \end{aligned} \quad (\text{B3})$$

Just letting $V = \begin{pmatrix} 1 & 0 & 0 \\ 0 & e^{-i\varphi_c} & 0 \\ 0 & 0 & e^{-i\varphi_p} \end{pmatrix}$, we have

$$\begin{aligned} V^\dagger H V &= \begin{pmatrix} 0 & \frac{\Omega_c}{2} & \frac{\Omega_p}{2} \\ \frac{\Omega_c}{2} & \Delta_c & 0 \\ \frac{\Omega_p}{2} & 0 & \Delta_p \end{pmatrix} \\ &\triangleq \bar{H}. \end{aligned} \quad (\text{B4})$$

By substituting Eq.(B2) and Eq.(B4) to Eq.(B3), we get

$$P_{|0\rangle\langle 0|} = |\langle 0| e^{-i\bar{H}t} |0\rangle|^2, \quad (\text{B5})$$

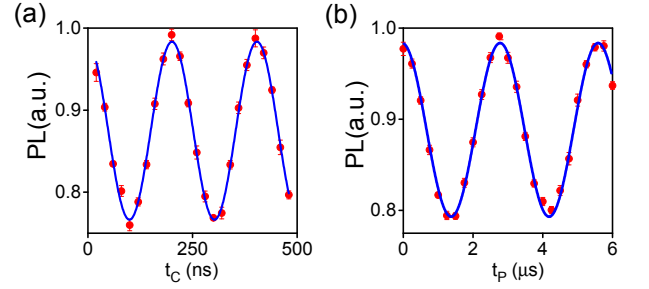


FIG. 8. (a)-(b) Rabi oscillation of the coupling and probe field for investigating dynamical process of ATS in main text Fig.3a-d and $\Omega_c/\Omega_p = 14$.

which means that the arbitrary initial phases of driving fields do not have any effect and can be neglected in the experiment.

2. The optimal demonstration of ATS

Now we chose the coupling field resonant with the single NV center. And in the dressed-state picture, Eq.(B2) (omitting the initial phases) can be expressed as

$$H_d = \begin{pmatrix} \frac{\Omega_c}{2} & 0 & \frac{\sqrt{2}\Omega_p}{4} \\ 0 & -\frac{\Omega_c}{2} & \frac{\sqrt{2}\Omega_p}{4} \\ \frac{\sqrt{2}\Omega_p}{4} & \frac{\sqrt{2}\Omega_p}{4} & \Delta_p \end{pmatrix}, \quad (\text{B6})$$

where $|+\rangle = \frac{|0\rangle+|1\rangle}{\sqrt{2}}$, $|-\rangle = \frac{|0\rangle-|1\rangle}{\sqrt{2}}$ and $|2\rangle = |2\rangle$ form new basis vectors. The frequency of the probe field was scanned to make sure that the Rabi frequency of probe field is 1/14 of that of the coupling field, as shown in Fig.8(a)-(b).

Case I: $\Delta_p = 0$, due to the large detuning between energy level of the NV center, the effect of the probe field can be neglected. The spin state is in bright state $|0\rangle$ when $\Omega_c t = 2n\pi, n = 1, 2, 3 \dots$, as shown in Fig.2(b) in the main text.

Case II: $\Delta_p \approx \frac{\Omega_c}{2}$, the middle energy level effect can be eliminated by the second order perturbation theory with

$$H_d = \begin{pmatrix} \frac{\Omega_c}{2} & 0 & \frac{\sqrt{2}\Omega_p}{4} \\ 0 & -\frac{\Omega_c}{2} & 0 \\ \frac{\sqrt{2}\Omega_p}{4} & 0 & \Delta_p + \frac{\Omega_p^2}{8\Omega_c} \end{pmatrix}. \quad (\text{B7})$$

So when the frequency of the probe field was scanned

and once $\Delta_p = \frac{\Omega_c}{2} - \frac{\Omega_p^2}{8\Omega_c}$, we have

$$\begin{aligned} P_{|0\rangle\langle 0|} &= \left| \frac{1}{\sqrt{2}} \begin{pmatrix} 1 & 1 & 0 \end{pmatrix} e^{-iH_d t} \frac{1}{\sqrt{2}} \begin{pmatrix} 1 \\ 1 \\ 0 \end{pmatrix} \right|^2 \\ &= \left| \frac{1}{\sqrt{2}} \begin{pmatrix} 1 & 1 & 0 \end{pmatrix} \frac{1}{\sqrt{2}} \begin{pmatrix} \cos \frac{\sqrt{2}\Omega_p t}{4} \\ e^{i\Omega_c t} \\ -i \sin \frac{\sqrt{2}\Omega_p t}{4} \end{pmatrix} \right|^2 \quad (\text{B8}) \\ &= \frac{1}{4} \left| \cos \frac{\sqrt{2}\Omega_p t}{4} + e^{i\Omega_c t} \right|^2. \end{aligned}$$

To get the highest contrast for the ATS, the conditions are:

$$\Omega_p t = 2\sqrt{2}(2k-1)\pi, \quad \Omega_c t = 2n\pi, \quad (\text{B9})$$

or

$$\Omega_p t = 2\sqrt{2}(2k)\pi, \quad \Omega_c t = (2n-1)\pi, \quad (\text{B10})$$

where $n, k = 1, 2, 3, \dots$.

Case III: $\Delta_p \approx -\frac{\Omega_c}{2}$, the situation is similar to Case II. So the conditions for the observation of the highest contrast is same and the resonance frequency of the probe field is $\Delta_p = -\frac{\Omega_c}{2} + \frac{\Omega_p^2}{8\Omega_c}$.

3. The ATS with non-resonant driving fields

For $\Omega_c \gg \Omega_p$, the ATS can be expressed as

$$\Delta_{AT} \approx \Omega_c - \frac{\Omega_p^2}{4\Omega_c} \approx \Omega_c. \quad (\text{B11})$$

If the coupling field is not resonant, we have

$$\begin{aligned} \bar{H} &= \frac{\Delta_c + \Omega_{eff}}{2} |+\rangle\langle +| + \frac{\Omega_c \Omega_p}{2\sqrt{2\Omega_{eff}^2 + 2\Delta_c \Omega_{eff}}} |+\rangle\langle 2| \\ &+ \frac{\Omega_c \Omega_p}{2\sqrt{2\Omega_{eff}^2 + 2\Delta_c \Omega_{eff}}} |2\rangle\langle +| + \frac{\Delta_c - \Omega_{eff}}{2} |-\rangle\langle -| \\ &+ \frac{\Omega_c \Omega_p}{2\sqrt{2\Omega_{eff}^2 - 2\Delta_c \Omega_{eff}}} |-\rangle\langle 2| \\ &+ \frac{\Omega_c \Omega_p}{2\sqrt{2\Omega_{eff}^2 - 2\Delta_c \Omega_{eff}}} |2\rangle\langle -| + \frac{\Delta_p}{2} |2\rangle\langle 2| \end{aligned} \quad (\text{B12})$$

in the bases of $|+\rangle = \frac{\Omega_c}{\sqrt{2\Omega_c^2 + 2\Delta_c^2 + 2\Delta_c \sqrt{\Omega_c^2 + \Delta_c^2}}} |0\rangle + \frac{\Delta_c + \sqrt{\Omega_c^2 + \Delta_c^2}}{\sqrt{2\Omega_c^2 + 2\Delta_c^2 + 2\Delta_c \sqrt{\Omega_c^2 + \Delta_c^2}}} |1\rangle$ and $|-\rangle = \frac{\Omega_c}{\sqrt{2\Omega_c^2 + 2\Delta_c^2 - 2\Delta_c \sqrt{\Omega_c^2 + \Delta_c^2}}} |0\rangle + \frac{\Delta_c - \sqrt{\Omega_c^2 + \Delta_c^2}}{\sqrt{2\Omega_c^2 + 2\Delta_c^2 - 2\Delta_c \sqrt{\Omega_c^2 + \Delta_c^2}}} |1\rangle$. Hence, when the two resonant transitions have non-zero detuning, the splitting exhibits asymmetric ATS (unequal transmission dips) and $\Delta_{AT} \approx \Omega_{eff} = \sqrt{\Omega_c^2 + \Delta_c^2}$.

4. The failure in the observation of ATS in a dephasing dominated system with traditional method

The traditional method to observe the ATS is based on the distribution of the population of static state under long-pulse driving fields [5–11, 15, 16, 18, 27], which can not be applied to demonstrate the ATS in the dephasing dominated system. Here, we employ Lindblad equation for the steady-state solution with

$$\dot{\rho}^I = -i[H_I, \rho^I] + \sum_j D(A_j^I) \rho^I, \quad (\text{B13})$$

where $D(A^I)\rho^I = A\rho^I A^\dagger - \{A^\dagger A, \rho^I\}/2$ and $H_I = \bar{H}$. The longitudinal relaxation from i to j can be written as $A_{diss} = \sqrt{\Gamma_{ij}}|j\rangle\langle i|$ and the dephasing process for state i is $A_{de} = \sqrt{2\gamma_a}|a\rangle\langle a|$.

For the dephasing channels,

$$D(A_{de})\rho = \begin{bmatrix} 0 & -\gamma_1\rho_{01} & -\gamma_2\rho_{02} \\ -\gamma_1\rho_{10} & 0 & -\gamma_3\rho_{12} \\ -\gamma_2\rho_{20} & -\gamma_3\rho_{21} & 0 \end{bmatrix}. \quad (\text{B14})$$

Just letting $\rho_{ij} \rightarrow \rho_{ij}^I$ for the expression of the dephasing process, we can transform the lab frame to the rotation frame.

In the NV center system, the dephasing process is much faster than the longitudinal relaxation ($\gamma \gg \Gamma$). So we can omit the longitudinal relaxation and get equation for the steady state after long-pulse driving,

$$0 = -i[H_I, \rho_I] + D(A_{de})\rho_I. \quad (\text{B15})$$

Hence, $\rho_{12}^I = \rho_{01}^I = \rho_{02}^I = 0$. At last,

$$\rho_{00}^I = \rho_{11}^I = \rho_{22}^I = \frac{1}{3}, \quad (\text{B16})$$

which means that the ATS or EIT cannot be observed with the traditional observation method. And it also holds for cascade and Λ three level system to investigate EIT or ATS based on the traditional observation method in the dephasing dominated quantum decoherence system.

5. The dynamical process of ATS and simulation

The dynamical process of ATS in NV center can also be numerically simulated with the Lindblad equation. The

independent equations of Eq.(B13) are

$$\begin{aligned}
\dot{\rho}_{00}^I &= -i \left[\frac{\Omega_c}{2} (\rho_{10}^I - \rho_{01}^I) + \frac{\Omega_p}{2} (\rho_{20}^I - \rho_{02}^I) \right], \\
\dot{\rho}_{01}^I &= -i \left[\frac{\Omega_c}{2} (\rho_{11}^I - \rho_{00}^I) + \frac{\Omega_p}{2} \rho_{21}^I \right] - \gamma_1 \rho_{01}^I, \\
\dot{\rho}_{02}^I &= -i \left[\frac{\Omega_c}{2} \rho_{12}^I + \frac{\Omega_p}{2} (\rho_{22}^I - \rho_{00}^I) - \Delta_p \rho_{02}^I \right] - \gamma_2 \rho_{02}^I, \\
\dot{\rho}_{11}^I &= -i \left[\frac{\Omega_c}{2} (\rho_{01}^I - \rho_{10}^I) \right], \\
\dot{\rho}_{12}^I &= -i \left[\frac{\Omega_c}{2} \rho_{02}^I - \frac{\Omega_p}{2} \rho_{10}^I - \Delta_p \rho_{12}^I \right] - \gamma_3 \rho_{12}^I, \\
1 &= \rho_{00}^I + \rho_{11}^I + \rho_{22}^I.
\end{aligned} \tag{B17}$$

The last equation is the additional constraint of completeness. Just letting

$$\begin{aligned}
\rho_{00}^I &= y_1, \\
\rho_{11}^I &= y_2, \\
\rho_{01}^I &= y_3 + iy_4, \\
\rho_{02}^I &= y_5 + iy_6, \\
\rho_{12}^I &= y_7 + iy_8,
\end{aligned} \tag{B18}$$

we can convert the physical equation to the linear ordinary differential equations and solve them with the Runge-Kutta method. The fluorescence intensity of the NV center is given by $I = 1 - C + Cy_1$ with $C = PL_{m_s=0} - PL_{m_s=\pm 1} = 0.22$ is fluorescence contrast for different spin states [39]. Fig.9(a) shows the result of the time dependence of the probabilities for a particular

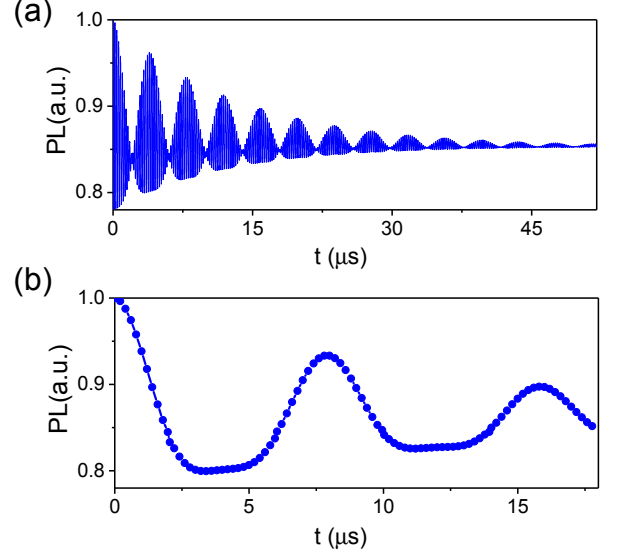


FIG. 9. (a)-(b) The result of the dynamical process of ATS shown with blue line based on solving the Lindblad equation. The parameters used in this figure are $\Omega_c = 5$ MHz, $\Omega_c/\Omega_p = 14$, $\gamma_1 = \gamma_2 = 0.0784$ MHz, $\gamma_3 = 2\gamma_2$, $\Delta_c = 0$, $\Delta_p = \frac{\Omega_c}{2} - \frac{\Omega_p^2}{8\Omega_c}$.

set of conditions beginning with $|0\rangle$. When the duration time of both driving fields is larger than the dephasing time, the system will become a maximally mixed state.

If the duration time of the driving fields satisfies $\Omega_c t = 2n\pi$ ($n = 1, 2, 3, \dots$), the envelope line will be obtained as shown in Fig.9(b). There is a little discrepancy between the theory and experimental result as shown in Fig.3(c) in the main text. The most important factors causing the deviation would be the environment treatment of NV center. For the present sample, the decoherence of NV center is dominated by the hyperfine interaction with the ^{13}C nuclear spins, which form a nuclear spin bath. The bath spins involved in the decoherence of NV center is much more complicated than those in quantum dots and shallow donors [46].

-
- [1] S. H. Autler and C. H. Townes, “Stark effect in rapidly varying fields,” *Phys. Rev.* **100**, 703–722 (1955).
 - [2] M. D. Lukin, “Colloquium: Trapping and manipulating photon states in atomic ensembles,” *Rev. Mod. Phys.* **75**, 457–472 (2003).
 - [3] M. Fleischhauer, A. Imamoglu, and J. P. Marangos, “Electromagnetically induced transparency: Optics in coherent media,” *Rev. Mod. Phys.* **77**, 633–673 (2005).
 - [4] A. Reiserer and G. Rempe, “Cavity-based quantum networks with single atoms and optical photons,” *Rev. Mod. Phys.* **87**, 1379–1418 (2015).
 - [5] M. J. Piotrowicz, C. McCormick, A. Kowalczyk, S. Bergamini, I. I. Beterov, and E. A. Yakshina, “Measurement of the electric dipole moments for transitions to rubidium Rydberg states via Autler–Townes splitting,” *New J. Phys.* **13**, 093012 (2011).
 - [6] E. H. Ahmed, S. Ingram, T. Kirova, O. Salihoglu, J. Huennekens, J. Qi, Y. Guan, and A. M. Lyyra, “Quantum control of the spin-orbit interaction using the Autler–Townes effect,” *Phys. Rev. Lett.* **107**, 163601 (2011).
 - [7] N. Timoney, I. Baumgart, M. Johanning, A. F. Varón, M. B. Plenio, A. Retzker, and Ch. Wunderlich, “Quantum gates and memory using microwave-dressed states,” *Nature* **476**, 185–188 (2011).
 - [8] X. Xu, Z. Wang, C. Duan, P. Huang, P. Wang, Y. Wang, N. Xu, X. Kong, F. Shi, X. Rong, and J. Du, “Coherence-protected quantum gate by continuous dynamical decoupling in diamond,” *Phys. Rev. Lett.* **109**, 070502 (2012).
 - [9] T. Van der Sar, Z. H. Wang, M. S. Blok, H. Bernien, T. H. Taminiau, D. M. Toyli, D. A. Lidar, D. D. Awschalom, R. Hanson, and V. V. Dobrovitski, “Decoherence-protected quantum gates for a hybrid solid-state spin register,” *Nature* **484**, 82–86 (2012).
 - [10] D. A. Golter, T. K. Baldwin, and H. Wang, “Protecting

- a solid-state spin from decoherence using dressed spin states,” *Phys. Rev. Lett.* **113**, 237601 (2014).
- [11] Y. He, Y. M. He, J. Liu, Y. J. Wei, H. Y. Ramírez, M. Atatüre, C. Schneider, M. Kamp, S. Höfling, C. Y. Lu, and J. W. Pan, “Dynamically controlled resonance fluorescence spectra from a doubly dressed single InGaAs quantum dot,” *Phys. Rev. Lett.* **114**, 097402 (2015).
 - [12] J. Zhang, P. W. Hess, A. Kyprianidis, P. Becker, A. Lee, J. Smith, G. Pagano, I. D. Potirniche, A. C. Potter, A. Vishwanath, N. Y. Yao, and C. Monroe, “Observation of a discrete time crystal,” *Nature* **543**, 217–220 (2017).
 - [13] M. Mücke, E. Figueroa, J. Bochmann, C. Hahn, K. Murr, S. Ritter, C. J. Villas-Boas, and G. Rempe, “Electromagnetically induced transparency with single atoms in a cavity,” *Nature* **465**, 755–758 (2010).
 - [14] J. Q. You and F. Nori, “Atomic physics and quantum optics using superconducting circuits,” *Nature* **474**, 589–597 (2011).
 - [15] M. A. Sillanpää, J. Li, K. Cicak, F. Altomare, J. I. Park, R. W. Simmonds, G. S. Paraoanu, and P. J. Hakonen, “Autler-Townes effect in a superconducting three-level system,” *Phys. Rev. Lett.* **103**, 193601 (2009).
 - [16] M. Baur, S. Filipp, R. Bianchetti, J. M. Fink, M. Göppl, L. Steffen, P. J. Leek, A. Blais, and A. Wallraff, “Measurement of Autler-Townes and Mollow transitions in a strongly driven superconducting qubit,” *Phys. Rev. Lett.* **102**, 243602 (2009).
 - [17] A. E. Miroshnichenko, S. Flach, and Y. S. Kivshar, “Fano resonances in nanoscale structures,” *Rev. Mod. Phys.* **82**, 2257–2298 (2010).
 - [18] M. Wagner, H. Schneider, D. Stehr, S. Winnerl, A. M. Andrews, S. Scharfner, G. Strasser, and M. Helm, “Observation of the intraexciton Autler-Townes effect in GaAs/AlGaAs semiconductor quantum wells,” *Phys. Rev. Lett.* **105**, 167401 (2010).
 - [19] E. Togan, Y. Chu, A. Imamoglu, and M. D. Lukin, “Laser cooling and real-time measurement of the nuclear spin environment of a solid-state qubit,” *Nature* **478**, 497–501 (2011).
 - [20] D. A. Golter, K. N. Dinyari, and H. Wang, “Nuclear-spin-dependent coherent population trapping of single nitrogen-vacancy centers in diamond,” *Phys. Rev. A* **87**, 035801 (2013).
 - [21] P. Jamonneau, G. Hétet, A. Dréau, J. F. Roch, and V. Jacques, “Coherent population trapping of a single nuclear spin under ambient conditions,” *Phys. Rev. Lett.* **116**, 043603 (2016).
 - [22] V. M. Acosta, K. Jensen, C. Santori, D. Budker, and R. G. Beausoleil, “Electromagnetically induced transparency in a diamond spin ensemble enables all-optical electromagnetic field sensing,” *Phys. Rev. Lett.* **110**, 213605 (2013).
 - [23] X. Yang, M. Yu, D. L. Kwong, and C. Wong, “All-optical analog to electromagnetically induced transparency in multiple coupled photonic crystal cavities,” *Phys. Rev. Lett.* **102**, 173902 (2009).
 - [24] B. Luk’yanchuk, N. I. Zheludev, S. A. Maier, N. J. Halas, P. Nordlander, H. Giessen, and C. T. Chong, “The Fano resonance in plasmonic nanostructures and metamaterials,” *Nat. Mater.* **9**, 707–715 (2010).
 - [25] C. Wu, A. B. Khanikaev, R. Adato, N. Arju, A. A. Yanik, H. Altug, and G. Shvets, “Fano-resonant asymmetric metamaterials for ultrasensitive spectroscopy and identification of molecular monolayers,” *Nat. Mater.* **11**, 69–75 (2012).
 - [26] J. Kim, M. C. Kuzyk, K. Han, H. Wang, and G. Bahl, “Non-reciprocal Brillouin scattering induced transparency,” *Nat. Phys.* **11**, 275–280 (2015).
 - [27] B. Peng, Ş. K. Özdemir, W. J. Chen, F. Nori, and L. Yang, “What is and what is not electromagnetically induced transparency in whispering-gallery microcavities,” *Nat. Commun.* **5**, 5082 (2013).
 - [28] G. Balasubramanian, P. Neumann, D. Twitchen, M. Markham, R. Kolesov, N. Mizuochi, J. Isoya, J. Achard, J. Beck, J. Tissler, *et al.*, “Ultralong spin coherence time in isotopically engineered diamond,” *Nat. Mater.* **8**, 383–387 (2009).
 - [29] Z. L. Xiang, S. Ashhab, J. Q. You, and F. Nori, “Hybrid quantum circuits: Superconducting circuits interacting with other quantum systems,” *Rev. Mod. Phys.* **85**, 623–653 (2013).
 - [30] E. Paladino, Y. M. Galperin, G. Falci, and B. L. Altshuler, “1/f noise: Implications for solid-state quantum information,” *Rev. Mod. Phys.* **86**, 361 (2014).
 - [31] D. J. Christle, A. L. Falk, P. Andrich, P. V. Klimov, J. U. Hassan, N. T. Son, E. Jánzén, T. Ohshima, and D. D. Awschalom, “Isolated electron spins in silicon carbide with millisecond coherence times,” *Nat. Mater.* **14**, 160–163 (2015).
 - [32] D. Suter and G. A. Álvarez, “Colloquium: Protecting quantum information against environmental noise,” *Rev. Mod. Phys.* **88**, 041001 (2016).
 - [33] B. M. Terhal, “Quantum error correction for quantum memories,” *Rev. Mod. Phys.* **87**, 307–346 (2015).
 - [34] D. A. Golter and H. Wang, “Optically driven Rabi oscillations and adiabatic passage of single electron spins in diamond,” *Phys. Rev. Lett.* **112**, 116403 (2014).
 - [35] C. Zu, W. B. Wang, L. He, W. G. Zhang, C. Y. Dai, F. Wang, and L. M. Duan, “Experimental realization of universal geometric quantum gates with solid-state spins,” *Nature* **514**, 72–75 (2014).
 - [36] G. Waldherr, Y. Wang, S. Zaiser, M. Jamali, T. Schulte-Herbrüggen, H. Abe, T. Ohshima, J. Isoya, J. F. Du, P. Neumann, *et al.*, “Quantum error correction in a solid-state hybrid spin register,” *Nature* **506**, 204–207 (2014).
 - [37] S. Choi, J. Choi, R. Landig, G. Kucsko, H. Zhou, J. Isoya, F. Jelezko, S. Onoda, H. Sumiya, V. Khemani, *et al.*, “Observation of discrete time-crystalline order in a disordered dipolar many-body system,” *Nature* **543**, 221–225 (2017).
 - [38] R. Hanson, V. V. Dobrovitski, A. E. Feiguin, O. Gywat, and D. D. Awschalom, “Coherent dynamics of a single spin interacting with an adjustable spin bath,” *Science* **320**, 352–355 (2008).
 - [39] X. D. Chen, L. M. Zhou, C. L. Zou, C. C. Li, Y. Dong, F. W. Sun, and G. C. Guo, “Spin depolarization effect induced by charge state conversion of nitrogen vacancy center in diamond,” *Phys. Rev. B* **92**, 104301 (2015).
 - [40] P. M. Anisimov, J. P. Dowling, and B. C. Sanders, “Objectively discerning Autler-Townes splitting from electromagnetically induced transparency,” *Phys. Rev. Lett.* **107**, 163604 (2011).
 - [41] Y. Dong, X. D. Chen, G. C. Guo, and F. W. Sun, “Reviving the precision of multiple entangled probes in an open system by simple π -pulse sequences,” *Phys. Rev. A* **94**, 052322 (2016).

- [42] G. Q. Liu, Y. R. Zhang, Y. C. Chang, J. D. Yue, H. Fan, and X. Y. Pan, “Demonstration of entanglement-enhanced phase estimation in solid,” *Nat. Commun.* **6**, 6726 (2015).
- [43] S. Arroyo-Camejo, A. Lazarev, S. W. Hell, and G. Balasubramanian, “Room temperature high-fidelity holonomic single-qubit gate on a solid-state spin,” *Nat. Commun.* **5**, 1 (2014).
- [44] C. G. Yale, F. J. Heremans, B. B. Zhou, A. Auer, G. Burkard, and D. D. Awschalom, “Optical manipulation of the Berry phase in a solid-state spin qubit,” *Nat. Photon.* **10**, 184–189 (2016).
- [45] Y. Sekiguchi, N. Niikura, R. Kuroiwa, H. Kano, and H. Kosaka, “Optical holonomic single quantum gates with a geometric spin under a zero field,” *Nat. Photon.* **11**, 309–314 (2017).
- [46] N. Zhao, S.-W. Ho, and R.-B. Liu, “Decoherence and dynamical decoupling control of nitrogen vacancy center electron spins in nuclear spin baths,” *Phys. Rev. B* **85**, 115303 (2012).